Internal versus external conductivity of a dense plasma: Many-particle theory and simulations

H. Reinholz*
University of Western Australia, School of Physics, 35 Stirling Highway, Crawley, WA 6009, Australia

I. Morozov
Institute for High Energy Densities of RAS, IHED-IVTAN, Izhorskaya, 13/19, Moscow 125412, Russia

G. Röpke and Th. Millat
University of Rostock, FB Physik, Universitätsplatz 3, D-18051 Rostock, Germany
(Received 17 October 2003; revised manuscript received 1 March 2004; published 15 June 2004)

In the long-wavelength limit $k=0$, the response function has been investigated with respect to the external and internal fields which is expressed by the external and internal conductivity, respectively. Molecular dynamics simulations are performed to obtain the current-current correlation function and the dynamical collision frequency which are compared with analytical expressions. Special attention is given to the dynamical collision frequency and the description of plasma oscillations in the case of $k=0$. The relation between the external and internal conductivity and the current-current correlation function is analyzed.

DOI: 10.1103/PhysRevE.69.066412 PACS number(s): 52.65.Yy, 52.27.Gr, 52.25.Mq, 71.45.Gm

I. INTRODUCTION

The treatment of strongly correlated Coulomb systems is a challenge for many-particle theories. It has applications in different fields such as dense ionic plasmas and the electron-hole plasma in excited semiconductors. Within a quantum statistical approach, the methods of equilibrium and nonequilibrium Green functions have successfully been utilized to calculate the properties of dense plasmas, see Ref. [1]. However, a problem is the validity of perturbative approximations when using the Green function approach for strongly correlated systems.

With increasing computer capacities, simulation techniques such as molecular dynamics (MD) simulations have been developed to obtain physical quantities from correlation functions, see Refs. [2–7]. The MD approach allows the application to large coupling parameters. On the other hand, quantum effects are difficult to include. This shortcoming is partially cured by considering pseudopotentials which effectively take into account the uncertainty principle by a short distance modification of the Coulomb interaction within the range of the thermal wavelength, see Ref. [1]. More rigorous methods to include quantum effects are wave packet MD simulations [8] or path integral Monte Carlo calculations [9].

Other points are the finite particle number and the limited accuracy when solving the equations of motion. The latter will not be discussed any further. The transition from a finite system to the thermodynamic limit of an infinite system can be performed by periodic boundary conditions. The total force on a given particle from all the other particles in a basic cell, as well as from the infinite array of their periodic images, can be obtained using the standard Ewald procedure [2,3].

In the present paper, the long-wavelength limit $\sigma(\omega) = \lim_{k\to 0}\sigma(k,\omega)$ of the dynamical conductivity is considered for a two-component plasma. According to the fluctuation-dissipation theorem (FDT), this transport quantity can be expressed in terms of equilibrium correlation functions, in particular the autocorrelation function (ACF) of the electrical current or the ACF of the electrical charge density. In the literature [3,10], see also Ref. [11], the internal as well as the external conductivity are introduced, relating the electrical current density to the internal or the external electrical field strength, respectively. We will present the corresponding relations in the following Sec. II. An important quantity related to the dynamical conductivity is the dynamical collision frequency $\nu(\omega)$. Analytical expressions can be derived in different approximations within a perturbative approach, see Ref. [12].

Section III defines the current ACF in the context of MD simulations, and the connection to the collision frequency is shown. While results from MD simulations and analytical approaches for the structure factor and other frequency dependent quantities at finite wave number k are in good agreement, see e.g. Refs. [2,7], we will discuss the zero-wave number case of MD simulations which is relevant for the dielectric function $\epsilon(k=0,\omega)$ or the dynamical conductivity $\sigma(\omega)$, see Sec. IV. Results for the current ACF and the dynamical collision frequency at parameter values of a strongly coupled plasma are shown.

The inclusion of a mean field when performing MD simulations is considered in Sec. V. Calculations are presented and compared with previous results. In both cases, the same dynamical collision frequency is obtained and compared with results of an analytical approach. With this, an apparent controversy between the internal and external conductivity in calculating the collision frequency is resolved. Conclusions are drawn in Sec. VI.

*Corresponding author. FAX: +49(0)381-498 6942;
Email address: heidi@physics.uwa.edu.au.

II. DYNAMICAL CONDUCTIVITY OF THE TWO-COMPONENT PLASMA

We consider a two-component fully ionized neutral plasma, such as a H plasma consisting of electrons and protons, at temperature T and particle density n of each component. The interaction of this Coulomb system is given by the Coulomb potential, and the plasma is characterizd by the nonideality parameter $\Gamma = e^2(4\pi n/3)^{1/3}(4\pi\epsilon_0 k_B T)^{-1}$ and the degeneracy parameter $\Theta = 2m_e k_B T\hbar^{-2}(3\pi^2 n)^{-2/3}$. The linear response to external perturbations in general is presented in various references, see, e.g., Refs. [1,12]. In the following, we will restrict ourselves to relations which are relevant for further discussion.

Under the influence of an external electric field $\vec{E}_{\rm ext}(\vec{r},t) = \vec{E}_0^{\rm ext} e^{i(\vec{k}\cdot\vec{r}-\omega t)}$ a longitudinal electrical current density $\langle \vec{J}_k \rangle^t$ is induced. If we consider the response in an isotropic system, the z axis can be selected without loss of generality in such a way that $\vec{E}_0^{\rm ext} = E_0^{\rm ext}\vec{e}_z$, $\vec{k} = k\vec{e}_z$, $\vec{J}_k = J_k^{\rm long}\vec{e}_z$. The relationship between the induced longitudinal current and the *external field* is given by the response function $\chi(k,\omega)$. Within linear response theory, $\chi(k,\omega)$ is related to the equilibrium correlation function of the longitudinal electrical current density [2,12]

$$\chi(k,\omega) = -i\beta\Omega_0 \frac{k^2}{\omega}\langle J_k^{\rm long}; J_k^{\rm long}\rangle_{\omega+i\eta} \tag{1}$$

$$= -i\beta\Omega_0 \frac{k^2}{\omega}\int_0^\infty dt e^{i(\omega+i\eta)t}\langle J_k^{\rm long}(t) J_k^{\rm long}\rangle, \tag{2}$$

where Ω_0 is the normalization volume. The brackets $\langle\cdots\rangle^t$ indicate taking the statistical average with the thermodynamic equilibrium distribution and the limit $\eta\to 0$ has to be taken after this averaging process. Since the longitudinal part of the current density is related to the charge density according to the balance equation (due to charge conservation), the longitudinal current ACF can also be expressed in terms of the charge density ACF.

According to the FDT, the response function is related to the dynamical structure factor or the longitudinal part of the dielectric tensor $\hat{\epsilon}(k,\omega)$ according to (c.f. [1,2,11,13])

$$\epsilon^{\rm long}(k,\omega) = 1 - \frac{\chi(k,\omega)}{\epsilon_0 k^2 + \chi(k,\omega)} = 1 - \frac{1}{\epsilon_0 k^2}\Pi^{\rm long}(k,\omega). \tag{3}$$

The longitudinal polarization function $\Pi^{\rm long}(k,\omega)$ gives the relation between the induced current and the *internal field* as does the dynamical conductivity

$$\sigma^{\rm long}(k,\omega) = \frac{i\omega}{k^2}\Pi^{\rm long}(k,\omega) = \frac{\epsilon_0\omega_{\rm pl}^2}{-i\omega + \nu(k,\omega)}. \tag{4}$$

It is also called the *internal conductivity* [10]. Via Eq. (4), the dynamical collision frequency $\nu(k,\omega)$ is defined by a generalized Drude formula where $\omega_{\rm pl} = (ne^2/\epsilon_0 m_{ei})^{1/2}$ is the plasma frequency and m_{ei} the reduced mass. The phenomenological Drude model is obtained from the generalized Drude formula, Eq. (4), if the collision frequency is considered to be a real constant equal to the inverse of the relaxation time τ in momentum phase space.

In analogy to the internal conductivity, a so-called *external conductivity* [3,10] can be introduced from the response function (1)

$$\sigma_{\rm ext}(k,\omega) = \frac{i\omega}{k^2}\chi(k,\omega) = \beta\Omega_0\langle J_k^{\rm long}; J_k^{\rm long}\rangle_{\omega+i\eta}. \tag{5}$$

This quantity is directly related to the longitudinal current ACF. Note that it is not the dynamical conductivity defined by Eq. (4). Instead, it is related to the dynamical collision frequency in the following way:

$$\sigma_{\rm ext}(k,\omega) = \frac{\epsilon_0\omega_{\rm pl}^2\omega}{-i(\omega^2 - \omega_{\rm pl}^2) + \omega\nu(k,\omega)}. \tag{6}$$

The transverse part of the dielectric tensor can also be related to a conductivity according to

$$\hat{\epsilon}(k,\omega) = 1 + \frac{i}{\epsilon_0\omega}\hat{\sigma}(k,\omega). \tag{7}$$

The transverse conductivity is defined in analogy to the longitudinal (4) as

$$\sigma^{\rm trans}(k,\omega) = \frac{i\omega}{k^2}\Pi^{\rm trans}(k,\omega) = \frac{\epsilon_0\omega_{\rm pl}^2}{-i\omega + \tilde{\nu}(k,\omega)}, \tag{8}$$

where $\tilde{\nu}(k,\omega)$ is commonly called memory function [2]. In principle, the investigation of the transverse conductivity requires the inclusion of the coupling to the transverse Maxwell fields in addition to the Coulomb interaction. Considering only Coulomb interactions, the Kubo-Greenwood formula [2–4,11,13,14] relates the polarization function directly to the transverse current ACF,

$$\sigma^{\rm trans}(k,\omega) = \beta\Omega_0\langle J_k^{\rm trans}; J_k^{\rm trans}\rangle_{\omega+i\eta}. \tag{9}$$

Within a Green function approach, a diagram representation is possible [12]. In contrast to $\chi(k,\omega)$ and the transverse polarization function, which are given by diagrams containing Coulomb interaction in any order, the respective current ACF $\Pi^{\rm long}(k,\omega)$ is given only by the irreducible diagrams. In the long-wavelength limit, transverse and longitudinal conductivities should lead to the same response of the system,

$$\sigma(\omega) = \lim_{k\to 0}\sigma^{\rm trans}(k,\omega) = \lim_{k\to 0}\sigma^{\rm long}(k,\omega). \tag{10}$$

This implies that the longitudinal and transverse current ACF for Coulomb systems behave differently in the long-wavelength limit as also pointed out in Ref. [3].

III. CURRENT AUTOCORRELATION FUNCTION

Within MD simulations [3,4,11,13], the normalized current ACF

$$K(t) = \frac{\langle J_k(t) J_k\rangle}{\langle J_k^2\rangle} \tag{11}$$

is calculated. Here, the long-wavelength limit ($k\to 0$) of the current

$$J_{k=0}(t) = \frac{1}{\Omega_0} \sum_c \sum_{i=1}^{N} e_c v_{i,c}^z(t) \tag{12}$$

is considered, where N is the number of electrons and singly ionized ions. At this stage it is not possible to distinguish between transverse and longitudinal components of the velocities. Due to isotropy, an arbitrary direction was chosen to be in z direction for the speed $v_{i,c}^z$ of the ith particle of component c, denoted by $\{i,c\}$. For convenience, we will drop the index k in the following. The normalizing factor is equal to

$$\langle J^2 \rangle = \frac{e^2}{3\Omega_0^2} N \langle v^2 \rangle = \frac{\epsilon_0 \omega_{\rm pl}^2}{\Omega_0 \beta}. \tag{13}$$

The Laplace transform of the current ACF reads

$$\langle J;J \rangle_{\omega + i\eta} = \langle J^2 \rangle \int_0^\infty e^{i(\omega + i\eta)t} K(t) dt. \tag{14}$$

On the basis of this quantity, two different results for the conductivity

$$\sigma(\omega) = \epsilon_0 \omega_{\rm pl}^2 \int_0^\infty e^{i(\omega + i\eta)t} K(t) dt \tag{15}$$

are derived depending on whether the current densities are considered to be long-wavelength limit of the longitudinal or transverse case.

First, within the transverse response, the Kubo-Greenwood formula (9) is utilized. The conductivity (15) is then related to the memory function $\tilde{\nu}(\omega)$ [2,4,13,14] via the Drude like formula (8) and we find

$$\frac{\tilde{\nu}(\omega)}{\omega_{\rm pl}} = \frac{\epsilon_0 \omega_{\rm pl}}{\sigma^{\rm trans}(\omega)} + i \frac{\omega}{\omega_{\rm pl}}. \tag{16}$$

If we assume a constant memory function (collision frequency) $\tilde{\nu}(\omega) = \tilde{\nu}$, the Laplace transformation of $\sigma^{\rm trans}(\omega)$ back to $K^{\rm trans}(t)$ using the functional dependence given by Eq. (15) leads to a monotonically decreasing $K^{\rm trans}(t) = \exp(-\tilde{\nu} t)$. This behavior is observed indeed in simulations for $\Gamma \leqslant 1$ [2,4,6,13,14].

Second, within longitudinal response, we have to distinguish between the external and the internal conductivity. Inserting Eqs. (14) and (13) into Eq. (5), this implies that expression (15) is the external conductivity. The internal conductivity can be calculated via

$$\sigma^{\rm long}(\omega) = \frac{\sigma_{\rm ext}(\omega)}{1 - i\sigma_{\rm ext}(\omega)/(\epsilon_0 \omega)} \tag{17}$$

and due to the generalized Drude formula (4) the collision frequency is, in contrast to Eq. (16),

$$\frac{\nu(\omega)}{\omega_{\rm pl}} = \frac{\epsilon_0 \omega_{\rm pl}}{\sigma_{\rm ext}(\omega)} + i \left(\frac{\omega}{\omega_{\rm pl}} - \frac{\omega_{\rm pl}}{\omega} \right). \tag{18}$$

Using a constant collision frequency $\nu(\omega) = \nu$ in the respective relationship (6) for the external conductivity, we find for the longitudinal current ACF via a Laplace transformation

$$K^{\rm long}(t) = \exp\left\{ -\frac{\nu}{2} t \right\} \left[-\frac{\nu}{2z} \sin(zt) + \cos(zt) \right], \tag{19}$$

$$z = \sqrt{\omega_{\rm pl}^2 - \frac{\nu^2}{4}}.$$

This shows that an oscillating behavior is expected for the ACF. The oscillation frequency tends to $\omega_{\rm pl}$ in the limit $\nu \to 0$.

In conclusion we find that the current ACF for the longitudinal and transverse response cannot be identical under the assumption that in the long-wavelength limit both $\nu(\omega)$ and $\tilde{\nu}(\omega)$ coincide. This should also be reflected in the actual procedure taken in the MD simulations. In the following Secs. IV and V we will resolve this apparent contradiction between the internal conductivity as obtained from the current ACF according to Eqs. (17) and (5) and the transverse conductivity obtained from the current ACF according to Eqs. (16) and (9).

IV. SIMULATION TECHNIQUE

In the MD simulation scheme, the Newtonian equations of motion are solved for a system consisting of N singly charged ions and N electrons exerting Coulomb forces on each other. The ith particle of component c shall be denoted as $\{i,c\}$. This is a classical treatment where the trajectories of each particle are determined. The original Coulomb interaction can be replaced by a pseudopotential, where the short-range part of the interaction is modified reflecting the quantum character of the interaction. A systematic derivation of a pseudopotential which reproduces the equilibrium properties has been given by Kelbg, see Refs. [1,15] on the basis of the Slater sum. In particular, we use the so-called "corrected Kelbg" potential [15]

$$V_{cd}(r) = \frac{e_c e_d}{4\pi\epsilon_0 r} \left[F\left(\frac{r}{\lambda_{cd}} \right) - r \frac{k_B T}{e_c e_d} \tilde{A}_{cd}(\xi_{cd}) \exp\left(-\left(\frac{r}{\lambda_{cd}} \right)^2 \right) \right], \tag{20}$$

where

$$\lambda_{cd} = \frac{\hbar}{\sqrt{2 m_{cd} k_B T}}, \quad \frac{1}{m_{cd}} = \frac{1}{m_c} + \frac{1}{m_d}, \quad \xi_{cd} = -\frac{e_c e_d}{k_B T \lambda_{cd}},$$

$$F(x) = 1 - \exp(-x^2) + \sqrt{\pi} x [1 - \mathrm{erf}(x)],$$

$$\tilde{A}_{ee}(\xi_{ee}) = \sqrt{\pi} |\xi_{ee}| + \ln\left[2\sqrt{\pi} |\xi_{ee}| \int_0^\infty \frac{y \exp(-y^2) dy}{\exp(\pi |\xi_{ee}| / y) - 1} \right],$$

$$\tilde{A}_{ei}(\xi_{ei}) = -\sqrt{\pi}\xi_{ei} + \ln\left[\sqrt{\pi}\xi_{ie}^3\left(\zeta(3) + \frac{1}{4}\zeta(5)\xi_{ie}^2\right) + 4\sqrt{\pi}\xi_{ei}\int_0^\infty \frac{y\,\exp(-y^2)dy}{1-\exp(-\pi\xi_{ei}/y)}\right],$$

where $\xi(n)$ are the Riemann-Zeta functions. This interaction potential corresponds to the Coulomb potential at large distances and provides the exact value of the Slater sum and its first derivative at $r=0$.

Initially, all the particles are gathered in a cubic box with the edge size L. The number of particles N in this basic cell is obtained from a given mean plasma density n via $N=nL^3$. To simulate an infinite homogeneous plasma, images of this charge-neutral basic cell are considered shifting the basic cell by integer multiples of L in different directions. This extended system has a constant mean plasma density n. Artefacts may occur due to the periodicity of the particle positions, but they are suppressed if the basic cell size is increased.

The dynamics of both electrons with charge $-e$, mass m_e and ions with charge e, mass m_i is considered. Because of the continuous expansion of such plasma, the nearest image method is applied to the force calculation procedure. Here, the force $\vec{F}_{i,c}=\vec{F}_{i,c}^{\,\mathrm{short}}+\vec{F}_{i,c}^{\,\mathrm{long}}$ on a particle $\{i,c\}$ is considered to consist of two contributions. The interaction forces between particle $\{i,c\}$ and the nearest neighbor images of all other particles found in the basic cell centered around the position $\vec{r}_{i,c}$ of the considered particle $\{i,c\}$ is the short-range contribution $\vec{F}_{i,c}^{\,\mathrm{short}}$. The contribution $\vec{F}_{i,c}^{\,\mathrm{long}}$ is originated from the remaining images, which are not in the basic cell.

The short-range part of the force is calculated as

$$\vec{F}_{i,c}^{\,\mathrm{short}} = \sum_d \sum_{j(\neq i)}^{N} \vec{F}_{cd}(\vec{r}_{\,j,d}^{\,\mathrm{n.n.}} - \vec{r}_{i,c}), \quad \vec{F}_{cd}(\vec{r}) = -\frac{\vec{r}}{r}\frac{dV_{cd}(r)}{dr}. \tag{21}$$

The time argument t is suppressed. According to this method it is assumed that the particle $\{i,c\}$ does not interact with original particles which at large t may be found far away due to the motion in space beyond the basic cell, but with their next neighbors' images obtained by periodically shifting their coordinates into the basic cell centered around the particle $\{i,c\}$. Thus, the position of each original particle $\vec{r}_{j,d}$ is replaced by the position of an image $\vec{r}_{\,j,d}^{\,\mathrm{n.n.}}$,

$$r_{j,d}^{\mathrm{n.n.},\alpha} = r_{j,d}^{\alpha} - mL, \quad \left|r_{j,d}^{\mathrm{n.n.},\alpha} - r_{i,c}^{\alpha}\right| \leqslant \frac{L}{2}, \tag{22}$$

where $\alpha=x,y,z$, and m is an integer. It should be noted that this procedure is repeated for each particle at $\vec{r}_{i,c}$. This method implies that each particle is always surrounded by $2N-1$ other particles with a constant mean density and the plasma is homogeneous in scales larger than the simulation cell.

The forces $\vec{F}_{i,c}^{\,\mathrm{long}}$ due to the interaction with images outside the basic cell centered around the position $\vec{r}_{i,c}$ of the particle $\{i,c\}$ are treated in a different way. If the dimension L of the basic cell is large in comparison to the screening length, the contributions of all images except the nearest one can be neglected. In particular, this is justified in the case of a nonideal plasma where the effective interaction potential decreases exponentially with distance due to screening. The influence of the far images can be taken into account considering Ewald sums. They are expected to give only a small contribution to the forces provided N is high enough. They do not change the behavior of the current ACF significantly and are not relevant with respect to our considerations.

For explicit MD simulations, we consider a model plasma consisting of singly charged ions and electrons with density $n=3.8\times10^{21}\mathrm{cm}^{-3}$ at a temperature of $T=33\ 000$ K. This corresponds to recent experiments in dense xenon plasmas [16]. The plasma parameters introduced in Sec. II take the value $\Gamma=1.28, \Theta=3.2$. It is a nondegenerate strongly coupled plasma. The computations of the current ACF for the ion-electron mass ratios $m_i/m_e=1836$ and $m_i/m_e=100$ show no considerable difference. Thus the ratio $m_i/m_e=100$ is selected for better convergence when averaging over the configurations of ions. The total number of particles $N=250$ was found to be enough for $\Gamma\approx1$. Further increase of the number of particles ($N=400$) does not affect any simulation results including the mean interaction energy, equilibrium correlation functions, and others. The equilibrium state of the plasma at the given temperature was obtained using a special procedure described in Ref. [5].

The current ACF is calculated directly from the velocities of the particles in subsequent time instances according to Eqs. (11) and (12), where $\Omega_0=L^3$ with L the length of the basic cell. The averaging of the ACF is performed over $(1-5)\times10^5$ initial configurations. These configurations are obtained from a long MD trajectory at different time moments. As shown in Ref. [6], two configurations are statistically independent if they are taken at times separated by the dynamical memory time. In our case about 5×10^3 initial configurations are already fully statistically independent for electrons. The dynamical memory time for ions increases with the ion mass [6]. Thus the smaller mass ratio the better averaging for ions is obtained.

Results are shown in Fig. 1 with circles. The current ACF $K(t)$ decreases monotonously as it was also obtained in previous MD simulations [2,4,6]. It indicates that the conductivity obtained numerically from $K(t)$ according to Eq. (15) should be treated as the transverse conductivity (8). The dimensionless dynamical conductivity $\sigma(\omega)/(\epsilon_0\omega_{\mathrm{pl}})$ is shown in Fig. 2 with circles. As $\omega\to0$, the real part has a finite value and the imaginary part vanishes, as expected from Eq. (16). According to the latter expression, we then deduct a memory function or collision frequency $\tilde{\nu}(\omega)$ as shown in Fig. 3 with circles.

The results of the MD simulations can be compared with analytical calculations. Details of different approximations for the dynamical collision frequency within a generalized linear response theory can be found in Ref. [12]. The dynamical collision frequency in Born approximation with respect to the statically screened potential (Debye potential) taken in the nondegenerate case and within the long-wavelength limit, is given here

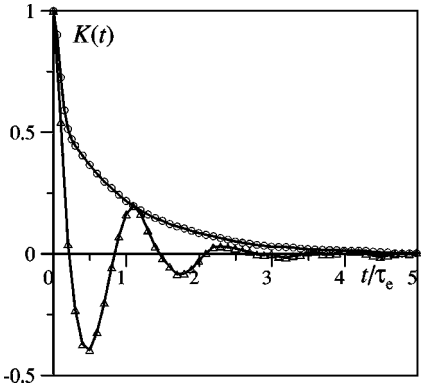

FIG. 1. Current autocorrelation function (ACF) for $\Gamma=1.28$, $m_i/m_e=100$; total number of averages 5×10^5; MD trajectory length of $2.5\times10^4\tau_e$, $\tau_e=2\pi/\omega_{pl}$ — period of electron plasma oscillations: MD simulations without (circles) and including (triangles) an additional mean-field term in the equations of motion.

$$\nu^{\mathrm{Born}}(k=0,\omega) = -ig\,n\int_0^\infty dy\,\frac{y^8}{(\bar{n}+y^2)^2}\left[\tilde{V}(q)\frac{16m_e k_B T\Omega_0\epsilon_0}{e^2\hbar^2}\right]^2 \times\int_{-\infty}^{\infty} dx e^{-(x-y)^2}\frac{1-e^{-4xy}}{xy(xy-\bar{\omega}-i\eta)}, \tag{23}$$

where

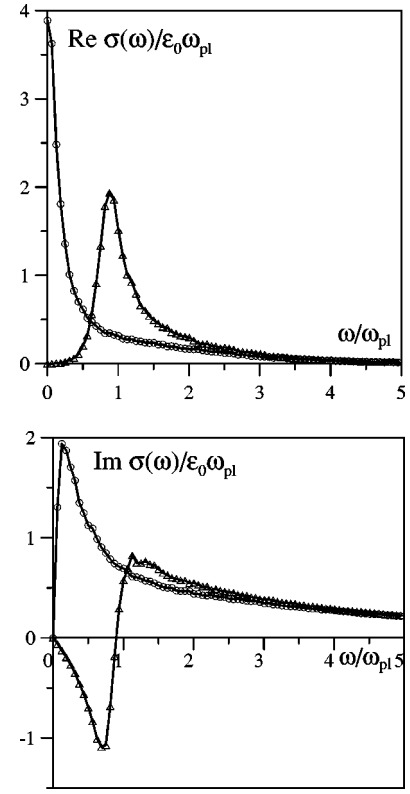

FIG. 2. Real and imaginary parts of the Laplace transformation of the current ACF; MD simulations without (circles) and including (triangles) an additional mean-field term in the equations of motion.

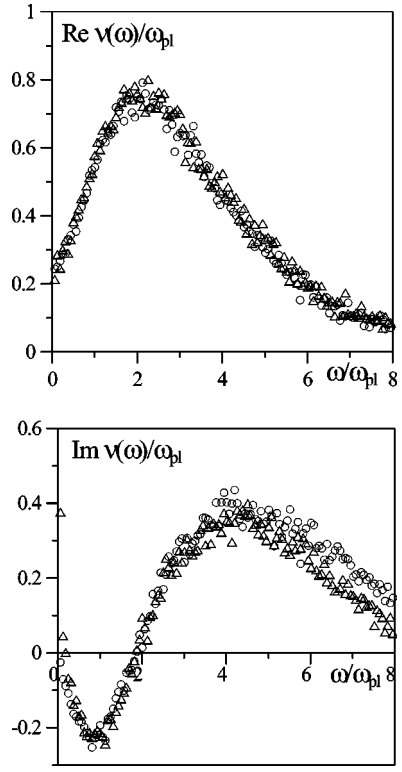

FIG. 3. Real and imaginary parts of the dynamic collision frequency or memory function from MD simulations without (circles) and including (triangles) an additional mean-field term in the equations of motion.

$$q=\frac{y}{\hbar}\sqrt{16m_e k_B T},\quad \bar{n}=\frac{\hbar^2 n e^2}{8\epsilon_0 m_e (k_B T)^2},$$
$$g=\frac{e^4\beta^{3/2}}{24\sqrt{2}\pi^{5/2}\epsilon_0^2 m_e^{1/2}},\quad \bar{\omega}=\frac{\hbar\omega}{4k_B T}. \tag{24}$$

In the case of the Fourier transform of the Coulomb interaction $\tilde{V}(q)=e^2/(\Omega_0\epsilon_0 q^2)$ the square brackets become $1/y^2$.

We will now compare the MD simulations with this analytical treatment of the dynamical collision frequency within perturbation theory, see Fig. 4. First, we consider a system with statically screened Coulomb interaction $\tilde{V}(q)=e^2/(\Omega_0\epsilon_0 q^2)$ according to Eq. (23). The results are presented as dotted line. The Born approximation can be improved by taking into account the effects of dynamically screening, strong collisions (T matrix), and higher moments by introducing a renormalization factor [12] in the generalized Drude formula, Eq. (4). This approximation is shown as solid line. Details of the calculation are given in Ref. [12]. It can be seen that both real and imaginary part are in good agreement with the simulation results for $\omega<\omega_{\mathrm{pl}}$. This means that in this region the quantum mechanical treatment of the Coulomb potential and the classical simulations based on the corrected Kelbg potential are consistent.

At frequencies $\omega\gg\omega_{\mathrm{pl}}$ the asymptotic expansion of the analytical expression for the collision frequency is possible

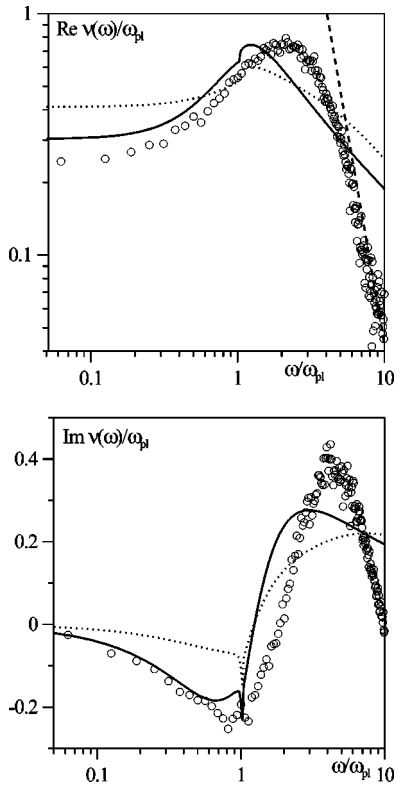

FIG. 4. Dynamical collision frequency within different methods; points — MD simulations; analytical approximations: dotted line — Born approximation, Eq. (23), with Coulomb potential, solid line — same approach including dynamically screening and strong collisions (T matrix) and higher moments via renormalization factor [12], dashed line — high frequency asymptote for Born approximation, Eq. (23), with corrected Kelbg potential.

using the Fourier transform of the corrected Kelbg potential (20)

$$\widetilde{V}_{cd}(q) = \frac{e_c e_d \lambda_{cd}}{\epsilon_0 \Omega_0 q}\left[\frac{\sqrt{\pi}}{\lambda_{cd}^2 q^2}\mathrm{erf}\left(\frac{\lambda_{cd}}{2}q\right)e^{-(\lambda_{cd}^2/4)q^2} - \frac{\lambda_{cd}^2 k_B T \pi^{3/2}\epsilon_0}{e_c e_d}\widetilde{A}_{cd}(\xi_{cd})q\; e^{-(\lambda_{cd}^2/4)q^2}\right]. \quad (25)$$

The high frequency behavior of the real part of the collision frequency is given in Fig. 4 as dashed line. It is found to behave as Re $\nu(\omega) \sim \omega^{-3.5}$. There is good agreement between the simulation data and the analytically derived high frequency behavior. The presented analytical treatment was also confirmed by MD calculations of the dynamical structure factor at finite k in Ref. [7] where the Deutsch potential was used. However, obviously the quantum Coulomb case is not well reproduced by a classical treatment using a pseudopotential based on Slater sums if the frequency is higher than the plasma frequency.

V. LONGITUDINAL CONDUCTIVITY

We now investigate the evaluation of the longitudinal conductivity by MD simulations. The current ACF K discussed in the preceding section has been identified as the transverse and cannot be taken as the longitudinal since they should behave differently as pointed out at the end of Sec. III and also in Ref. [3]. Therefore, the current ACF K^{long} has to be calculated differently to the ACF K^{trans}. It will be shown in which way the simulations have to be altered in order to obtain the longitudinal current ACF in the long-wavelength limit. However, we note that for finite wave vector k the condition $k > 2\pi/L$ means that any charge density wave occurs already within the basic simulation cell and the corresponding mean electric field is accurately taken into account. Excellent agreement for the dynamical structure factor from MD simulations and analytical expressions has been found [7]. The limit $k \to 0$ is not trivial. For any small k, the system is nearly homogeneous, but charge densities (or surface densities) are present at large distances, which can also be considered as a mean field.

For this, we follow the procedure to construct an infinite system by periodic images of a basic cell. We consider this as a limiting case of a finite number of images. Denoting the images in z direction by N_{images}, then a surface of our system is obtained at $z_- = -(N_{\mathrm{images}}+1)L/2$ and $z_+ = (N_{\mathrm{images}}+1)L/2$. When considering the force calculation procedure, there are contributions to the forces originating from a surface charge density. This occurs if positive and negative charges are moving at different rates across the surface of the basic cell. The introduction of a finite number of images compensates this effect at the interfaces, but not at the surface of the whole system including all the images. A large dipole moment follows connected with a finite polarization of the system. This surface charge density will produce an electrical field which has to be taken into account even in the limit when the number of images goes to infinity. If the surface is far away, it produces a homogeneous electrical field $\vec{E}(t)$ within the simulation box. Following this reasoning, it is necessary to include a mean field in the long-wavelength limit as shown below. As a consequence, plasma oscillations are obtained in the current ACF.

On the macroscopic level, the Maxwell equations relate this mean field $\vec{E}(t)$ to the average current density $\vec{J}(t)$, which is oriented in z direction according to the conventions in Sec. II,

$$\frac{d\vec{E}(t)}{dt} = -\frac{1}{\epsilon_0}\langle \vec{J}(t)\rangle. \quad (26)$$

Taking the current density according to Eq. (12) as an average over all original charged particles in the basic simulation cell and the initial condition $\vec{E}(0)=0$, the integration of Eq. (26) leads to

$$\vec{E} = \frac{1}{L^3}\left(-e\sum_{i=1}^{N}\vec{r}_{i,e} + e\sum_{i=1}^{N}\vec{r}_{i,i}\right). \quad (27)$$

In this approach, a contribution to the long-range interaction forces is given by $\vec{F}_{i,c}^{\mathrm{long}}(t) = e_c\vec{E}(t)$. In particular, the equation of motion includes two parts

$$m_c \frac{d\vec{v}_{i,c}}{dt} = \vec{F}_{i,c}^{\text{short}} - e_c \vec{E}. \tag{28}$$

The interaction forces $\vec{F}_{i,e}^{\text{short}}$ originate from close partners in the Debye sphere within the basic cell. It is fluctuating around a nearly zero mean value. Nevertheless, the amplitude of these fluctuations is much higher than the fluctuations of $e\vec{E}$. The Maxwell field (26) originates from all charged particles in the basic cell so that F^{long} is also produced by particles outside the Debye sphere. In contrast to the Ewald sum, this term gives rise to plasma oscillations as shown below.

In the MD method, if no mean-field term is taken into account, the total energy

$$\mathcal{E}_{\text{tot}} = \mathcal{E}_{\text{pot}} + \mathcal{E}_{\text{kin}} = \frac{1}{2}\sum_{c,d}\sum_{\substack{i,j \\ i\neq j}}^{N} V_{cd}(\vec{r}_{j,d} - \vec{r}_{i,c}) + \frac{m_e}{2}\sum_{i=1}^{N} v_{i,e}^2 + \frac{m_i}{2}\sum_{i=1}^{N} v_{i,i}^2 \tag{29}$$

is conserved. If the particle trajectories are calculated including the mean-field force, the energy $\mathcal{E}'_{\text{pot}} + \mathcal{E}'_{\text{kin}}$ is not conserved. Nevertheless, the conservation law can be fulfilled by including the mean-field energy $\mathcal{E}_{\text{field}} = L^3 \epsilon_0 E^2/2$ so that the total energy $\mathcal{E}'_{\text{tot}} = \mathcal{E}'_{\text{pot}} + \mathcal{E}'_{\text{kin}} + \mathcal{E}_{\text{field}}$ is conserved. This is illustrated by simulations below.

The occurrence of plasma oscillations can be demonstrated in the following way. If the mass ratio between electrons and ions m_i/m_e is large the ion current can be neglected in Eq. (12). After that the derivative of the total current density is obtained from

$$\frac{d\vec{J}(t)}{dt} = -\frac{e}{L^3}\sum_{i=1}^{N}\frac{d\vec{v}_i}{dt} = \frac{eN}{mL^3}(e\vec{E} - \vec{\xi}), \tag{30}$$

$$\vec{\xi} = \frac{1}{N}\sum_{i=1}^{N}\vec{F}_{i,e}^{\text{short}} = \frac{1}{N}\sum_{i=1}^{N}\sum_{j=1}^{N}\vec{F}_{ij}. \tag{31}$$

The force $\vec{\xi}$ includes only electron-ion interaction forces as all electron-electron interaction forces are compensated since they do not change the total momentum of the electrons. Although the force $\vec{F}_{i,e}^{\text{short}}$ on each electron is typically much greater than the force $e\vec{E}$ from the mean electric field, the average over all electrons is of the same order of magnitude as $e\vec{E}$. If we now differentiate Eq. (26) and substitute the derivative of the current using Eq. (30), we obtain the equation for the mean field

$$\frac{d^2\vec{E}}{dt^2} + \omega_{\text{pl}}^2 \vec{E} = \frac{\omega_{\text{pl}}^2}{e}\vec{\xi}. \tag{32}$$

On an average, $\vec{\xi}$ vanishes, so that plasma oscillations are described. The corresponding oscillations in the current ACF are obtained from MD simulations as the results below show.

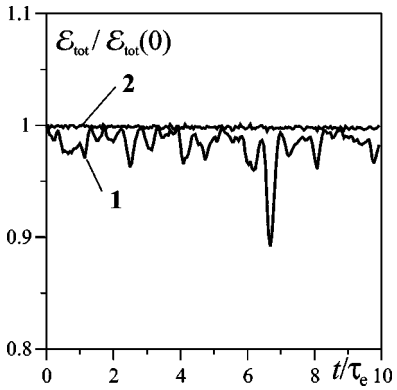

FIG. 5. Conservation of the total energy in MD simulations; curve **1** — total energy of the particles $\mathcal{E}'_{\text{pot}} + \mathcal{E}'_{\text{kin}}$ according to Eq. (29), curve **2** — total energy $\mathcal{E}'_{\text{tot}}$ including the mean-field energy.

We now present MD simulations based on the solution of the equations of motion (28) in comparison to the MD simulations as presented in Sec. IV where the contribution of the mean field $-e\vec{E}$ was not taken into account. The energy conservation is demonstrated in Fig. 5 according to Eq. (29). It can also be seen that the field energy $\mathcal{E}_{\text{field}}$ is rather small compared to the particle energy $\mathcal{E}'_{\text{pot}} + \mathcal{E}'_{\text{kin}}$.

Results for the longitudinal and transverse current ACF are shown in Fig. 1. After including the mean field into the MD simulations, the plasma oscillations in $K(t)$ become well pronounced in contrast to a monotonously decreasing behavior. It should be stressed that the amplitude of these oscillations does not depend on N.

The conductivity calculated according to Eq. (15) is shown in Fig. 2. In comparison to the transverse case, the conductivity shows a qualitatively different behavior. The real part following from the MD simulations including mean field is zero for zero frequency as is expected from the expression for the external conductivity (6). For the case without mean field, Re σ has a finite value. In the high frequency limit, both curves coincide. The dynamical collision frequencies $\nu(\omega)$ and the memory function $\tilde{\nu}(\omega)$ calculated from the simulation data for the ACFs are shown in Fig. 3. As pointed out, the results for the Laplace transform of the ACF differ significantly (Fig. 2). Nevertheless, if Eq. (18) is used for the collision frequency $\nu(\omega)$ and Eq. (16) for the memory function $\tilde{\nu}(\omega)$ in order to calculate the collision frequency, the results for both coincide quite clearly (Fig. 3). The difference between Im $\nu(\omega)$ and Im $\tilde{\nu}(\omega)$ in the low frequency limit is caused by the numerical error of Im $\nu(\omega)$ due to subtraction of two large terms in Eq. (18).

Therefore, our analysis showed that the apparent contradiction between the transverse conductivity which should be identical with the internal conductivity in the long-wavelength limit and the external conductivity could be resolved if the simulations for the transverse and longitudinal current ACF are carried out differently.

VI. CONCLUSION

Molecular dynamics simulations of strongly coupled plasmas were performed using the quasiclassical Kelbg interac-

tion potential. The current autocorrelation function was computed for a nondegenerate two-component plasma. Whereas for finite k the dynamical structure factor and the plasma oscillations are reproduced by MD simulations, see Refs. [2,4,7], the original methods do not allow to consider k values with $k<2\pi/L$. On the other hand $k=0$ should be possible to investigate with MD simulations in a finite volume.

We presented calculations for the transverse current ACF as well as for the longitudinal one. Although in the limit $k \to 0$ the transverse and longitudinal dielectric function and conductivities, respectively, coincide, the current ACF behave differently in this limiting case. It was shown that the results of MD simulations without a mean field in the long-wavelength limit provide the monotonously decreasing transverse ACF. Its Laplace transform is to be directly related to the transversal conductivity.

In MD simulations for the longitudinal case, a mean-field term has to be included into the equations of motion in addition to the short-range forces inside the Debye sphere. This mean-field term originates from surface charges not taken into account in the usual procedure of force calculation by the nearest image method. Simulations with these altered equations of motion show well pronounced plasma oscillations in the longitudinal current ACF. The results for the collision frequency as obtained in both simulation methods using the corresponding relations for the internal or external conductivities do coincide.

Additionally, the dynamical collision frequency inferred from the simulation data was compared with analytical results, which were derived using a generalized linear response theory. We found good agreement in the low and high frequency limits for a moderate nonideality. In particular, for $\omega<\omega_{\mathrm{pl}}$, classical MD simulations using the corrected Kelbg potential are able to reproduce the quantum behavior of Coulomb plasmas.

ACKNOWLEDGMENTS

The authors are thankful to G.E. Norman, A.A. Valuev, and G. Zwicknagel for fruitful discussions. I.M. acknowledges the support from RFBS by Grant No. 03-07-90272v, Integracia by Grants Nos. U0022, I0661, the Dynasty Foundation and the International Center of Fundamental Physics in Moscow. H.R. was financially supported by the DFG and T.M. was supported by the SFB 198.

[1] W.-D. Kraeft, D. Kremp, W. Ebeling, and G. Röpke, *Quantum Statistics of Charged Particle System* (Plenum, New York, Akademie Verlag, Berlin, 1986).

[2] J. P. Hansen and I. R. McDonald, Phys. Rev. A **23**, 2041 (1981); L. Sjögren, J. P. Hansen, and E. L. Pollock, *ibid.* **24**, 1544 (1981).

[3] J. P. Hansen and I. R. McDonald, *Theory of simple liquids* (London, Academic Press, 1976).

[4] J. P. Hansen, in *Strongly Coupled Plasma Physics*, edited by F. J. Rogers and H. E. DeWitt (Plenum, New York, 1987), p. 111.

[5] I. V. Morozov, G. E. Norman, and A. A. Valuev, Dokl. Akad. Nauk **362**, 752 (1998); Dokl. Phys. **43**, 608 (1998).

[6] I. V. Morozov, G. E. Norman, and A. A. Valuev, Phys. Rev. E **63**, 036405 (2001).

[7] A. Selchow, G. Röpke, A. Wierling, H. Reinholz, T. Pschiwul, and G. Zwicknagel, Phys. Rev. E **64**, 056410 (2001).

[8] D. Klakow, C. Toepffer, and P.-G. Reinhard, J. Chem. Phys. **101**, 10 766 (1994); M. Knaup, P.-G. Reinhard, and C. Toepffer, Contrib. Plasma Phys. **41**, 159 (2001).

[9] B. Millitzer and S. M. Ceperley, Phys. Rev. Lett. **85**, 1890 (2000).

[10] V. M. Adamyan, T. Meier, and I. M. Tkachenko, Fiz. Plazmy **11**, 826 (1985); V. M. Rylyuk and I. M. Tkachenko, Phys. Rev. A **44**, 1287 (1991).

[11] G. D. Mahan, *Many-Particle Physics* (Plenum, New York, 1990).

[12] H. Reinholz, R. Redmer, G. Röpke, and A. Wierling, Phys. Rev. E **62**, 5648 (2000).

[13] S. Ichimaru, *Statistical Plasma Physics*, Basic Principles Vol. I (Addison-Wesley, Reading, 1992).

[14] R. Kubo, M. Toda, and N. Hashitsume, *Statistical Physics II* (Springer, Berlin, 1985).

[15] W. Ebeling, G. E. Norman, A. A. Valuev, and I. A. Valuev, Contrib. Plasma Phys. **39**, 61 (1999).

[16] H. Reinholz, Yu. Zaporoghets, V. Mintsev, V. Fortov, I. Morozov, and G. Röpke, Phys. Rev. E **68**, 036403 (2003).